US 20060063995A1

(19) United States

(12) Patent Application Publication (10) Pub. No.: US 2006/0063995 A1

Yodh et al. (43) Pub. Date: Mar. 23, 2006

(54) OPTICAL MEASUREMENT OF TISSUE BLOOD FLOW, HEMODYNAMICS AND OXYGENATION

(75) Inventors: **Arjun G. Yodh**, Merion, PA (US); **Joel H. Greenberg**, Wayne, PA (US); **Guoqiang Yu**, Flemington, NJ (US); **John A. Detre**, Wynnewood, PA (US); **Turgut Durduran**, Upper Darby, PA (US); **Mark G. Burnett**, Philadelphia, PA (US); **Emile R. Mohler III**, Radnor, PA (US); **Harry Quon**, Rose Valley, PA (US); **Stephen M. Hahn**, Glen Mills, PA (US)

Correspondence Address:
WOODCOCK WASHBURN LLP
ONE LIBERTY PLACE, 46TH FLOOR
1650 MARKET STREET
PHILADELPHIA, PA 19103 (US)

(73) Assignee: **Trustees of the University of Pennsylvania**, Philadelphia, PA

(21) Appl. No.: **11/106,390**

(22) Filed: **Apr. 13, 2005**

Related U.S. Application Data

(60) Provisional application No. 60/561,758, filed on Apr. 13, 2004.

Publication Classification

(51) **Int. Cl.**
A61B 5/00 (2006.01)
A61B 5/02 (2006.01)

(52) **U.S. Cl.** **600/323**; 600/504

(57) **ABSTRACT**

An embodiment of the invention includes a device, system and method for determining the characteristics of deep tissue. The novel method includes measuring blood flow rate and oxygenation characteristics of the tissue, and determining oxygen metabolism of the tissue as a function of the measure blood flow rate and measure oxygenation. The blow flow rate characteristics are measured as a function of light fluctuations caused by the tissue, while the oxygenation characteristics are measured as a function of transmission of light through the tissue with respect to the wavelength of light. The tissue may be layered tissue, for example, a portion of a brain. The tissue characteristics may be measured during times of varying levels of exercise intensity.

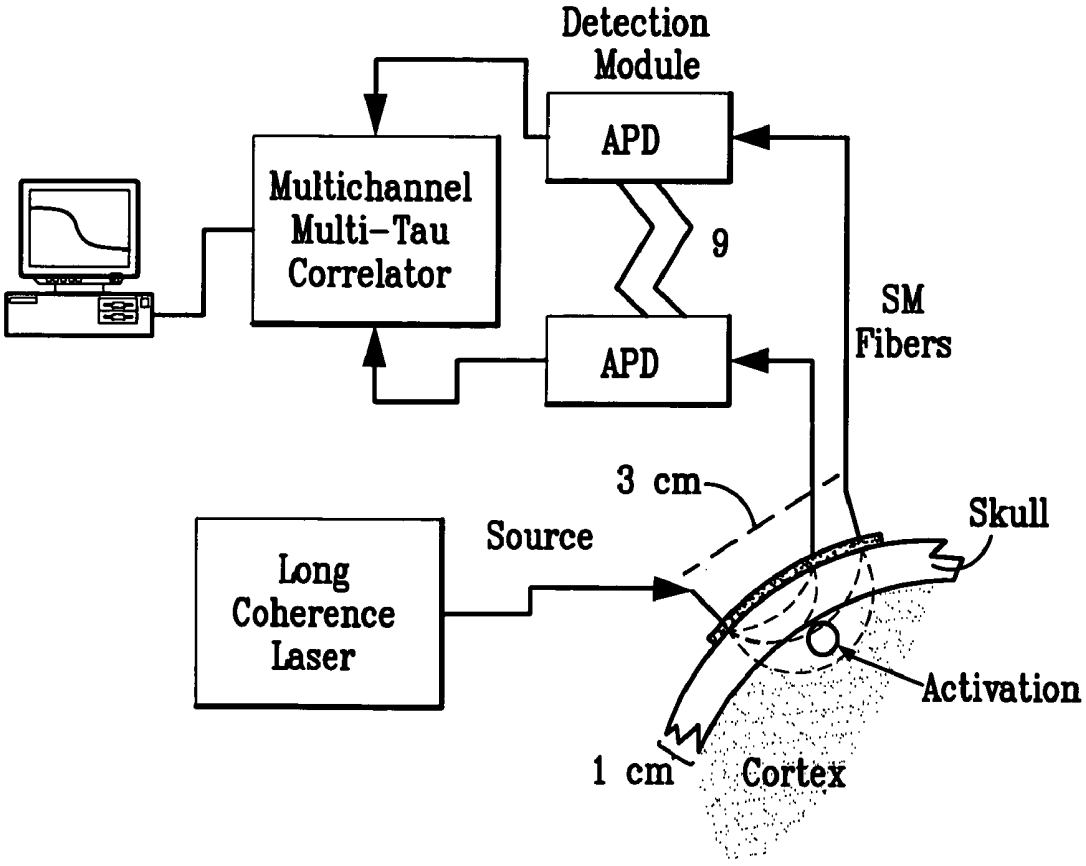

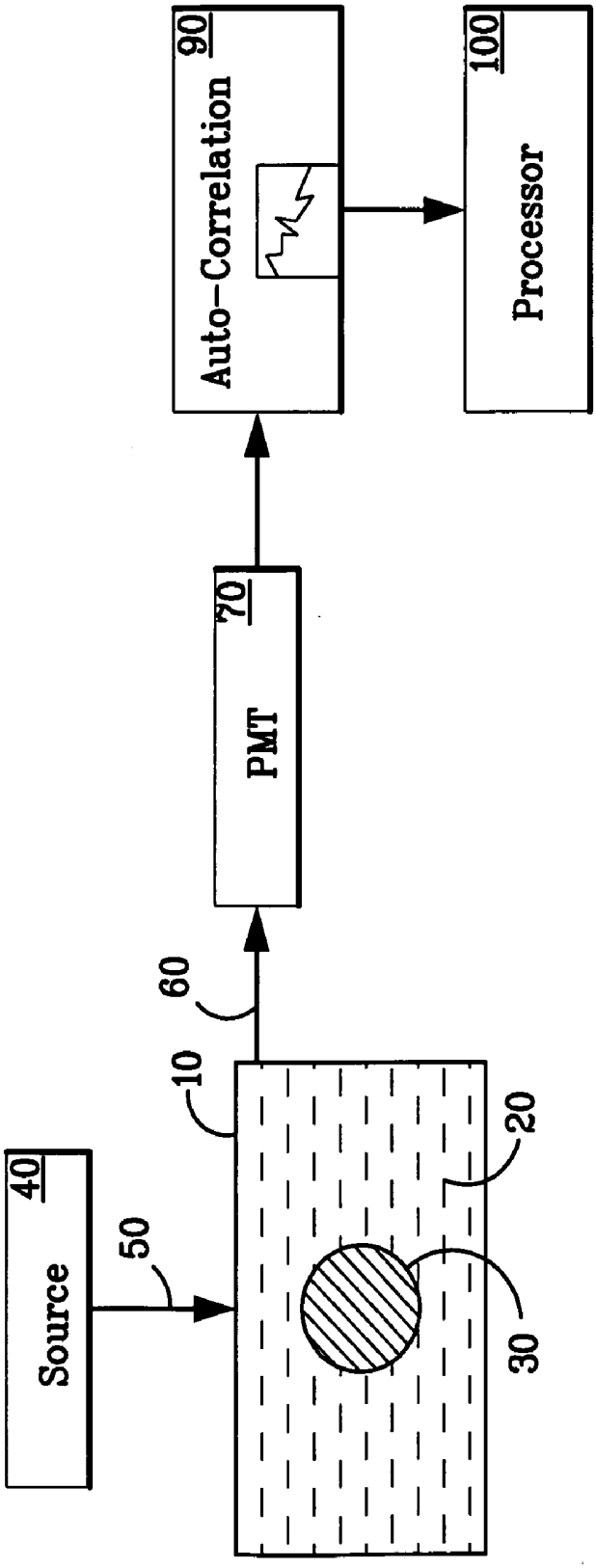
90
Auto-Correlation
100
Processor
70
PMT
60
10
20
40
Source
50
30

FIG. 1

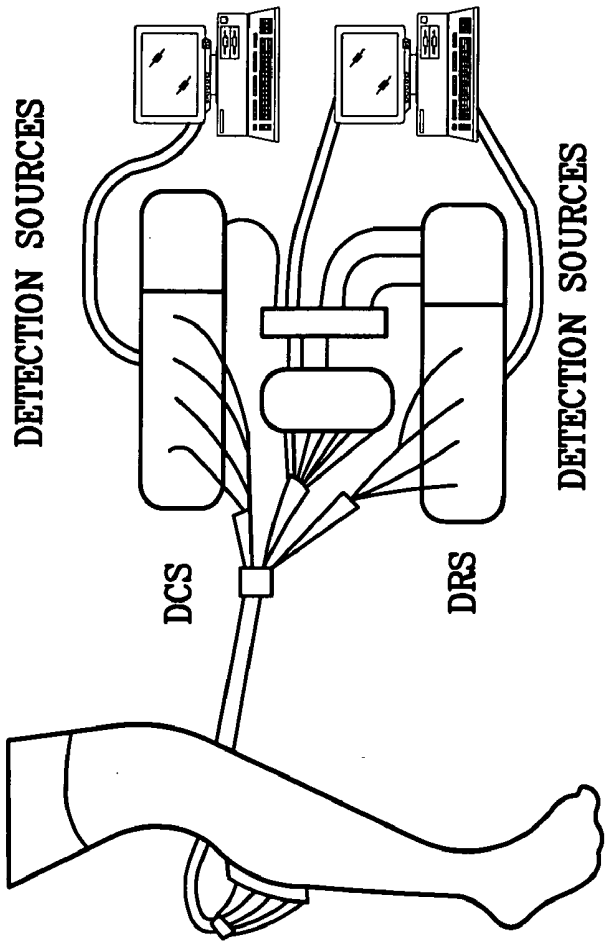

FIG. 2

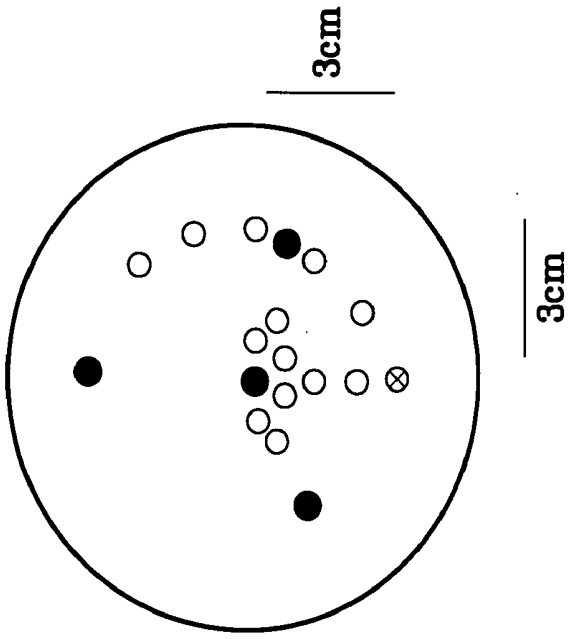

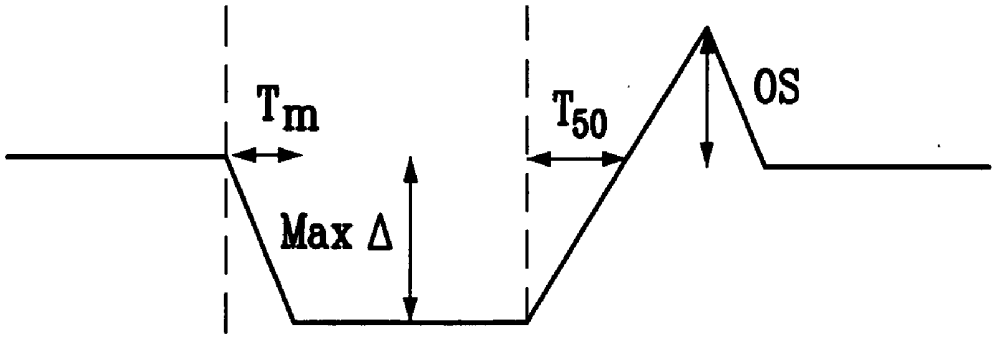

FIG. 3

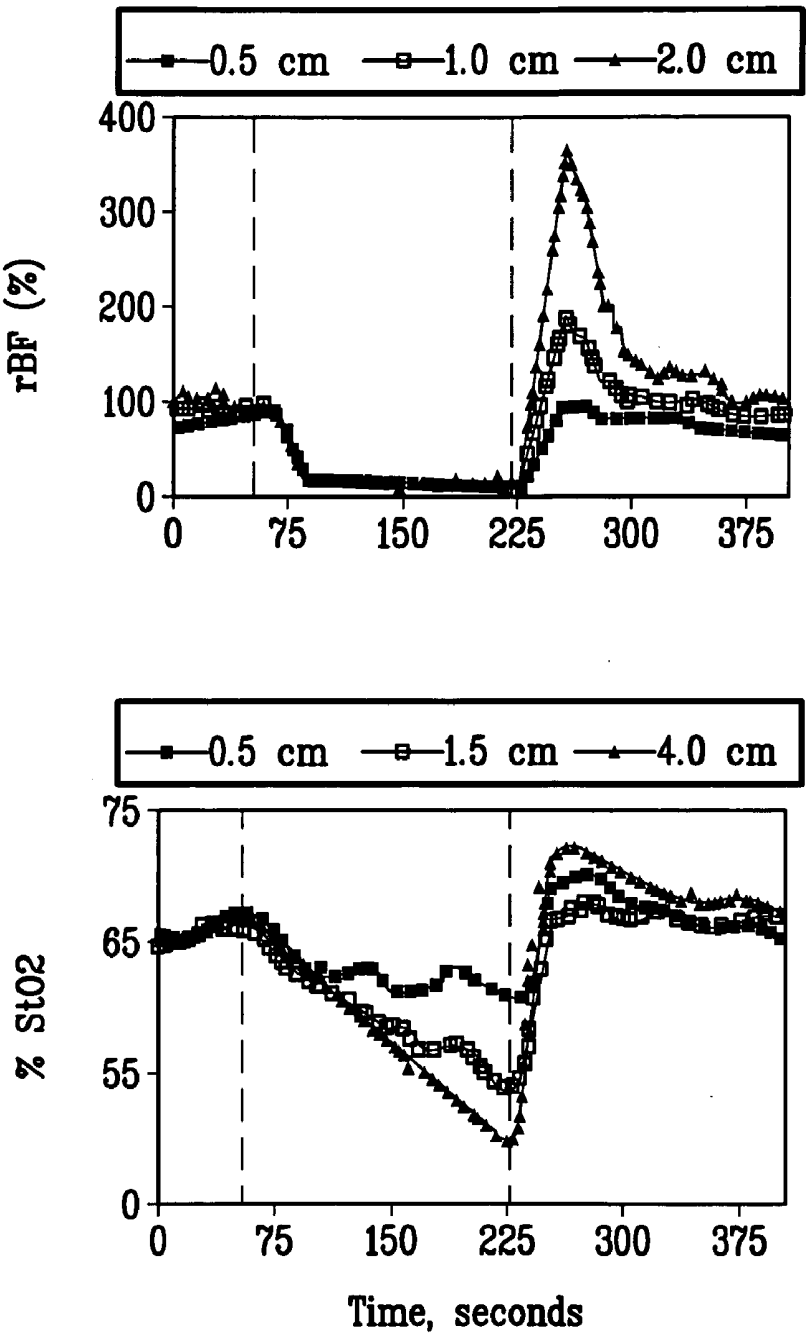
0.5 cm
1.0 cm
2.0 cm
rBF (%)
400
300
200
100
0
0
75
150
225
300
375
0.5 cm
1.5 cm
4.0 cm
% StO2
75
65
55
0
0
75
150
225
300
375
Time, seconds

FIG. 4

FIG. 5

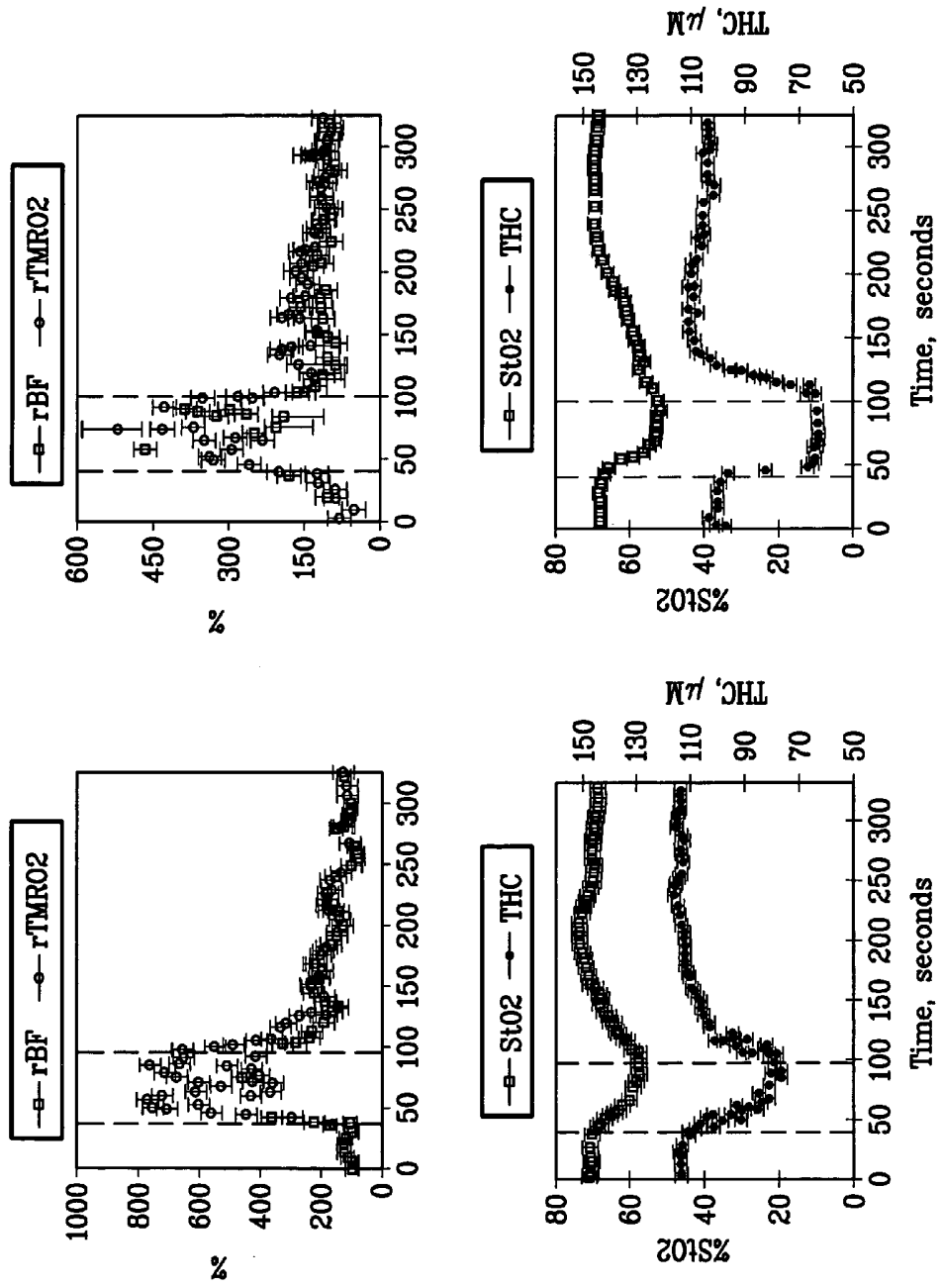

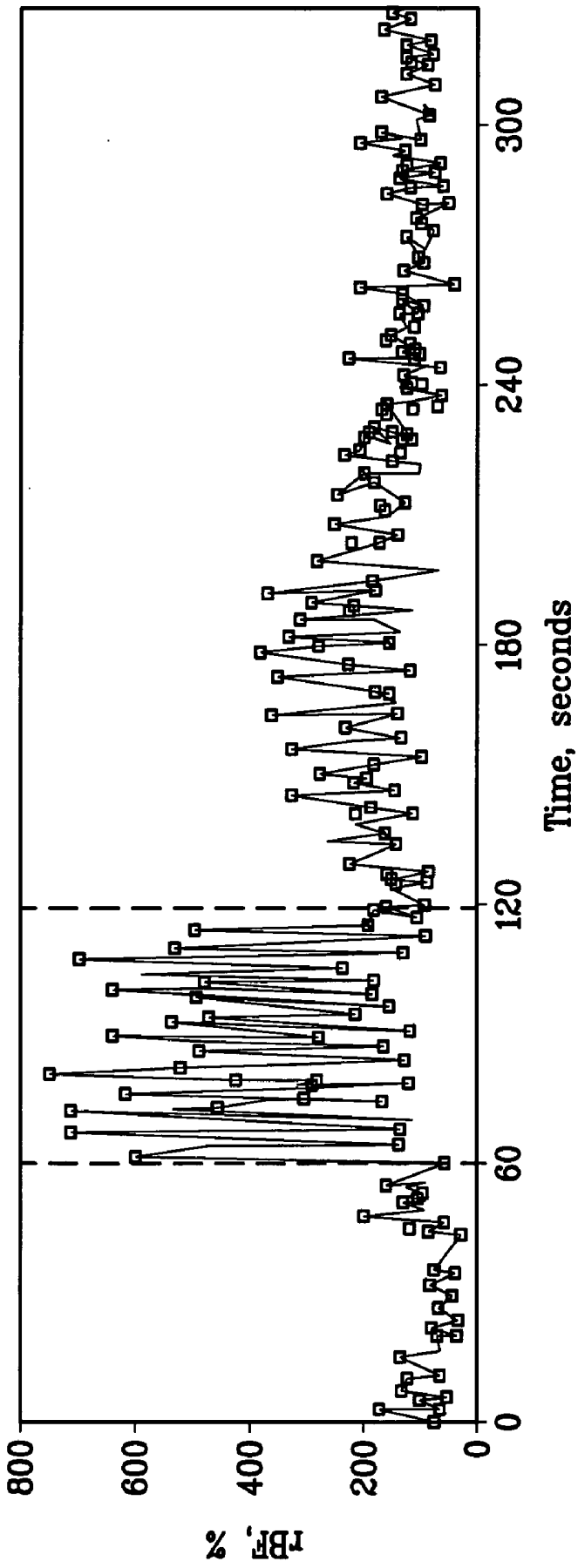

FIG. 6

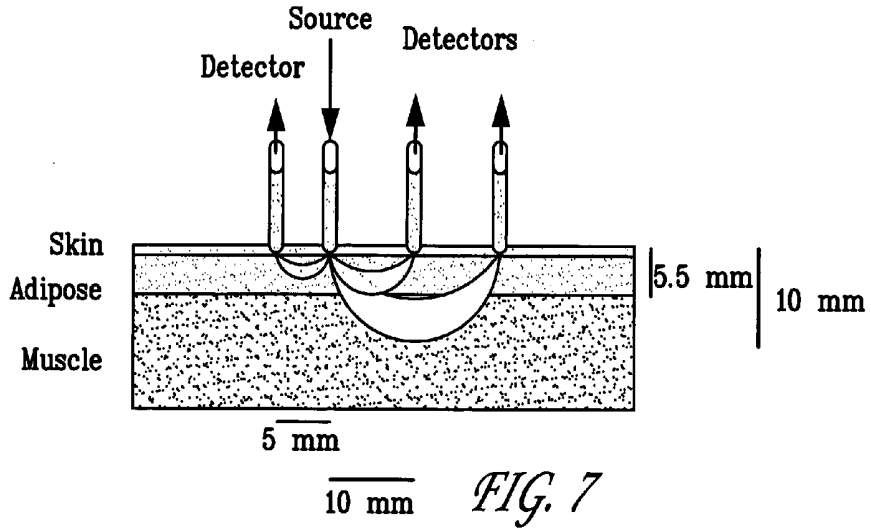
Source
Detector
Detectors
Skin
Adipose
Muscle
5.5 mm
10 mm
5 mm
10 mm

FIG. 7

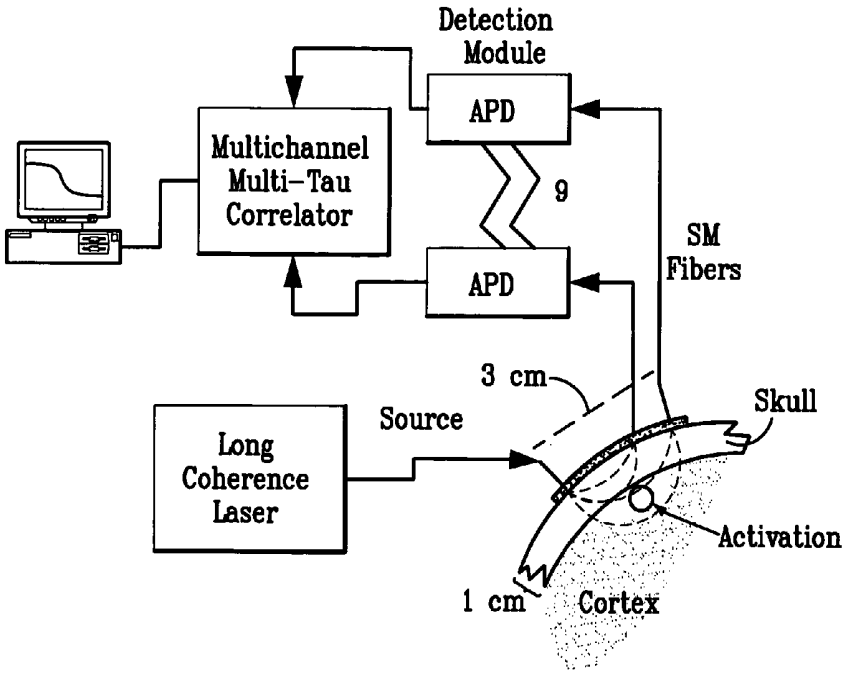
Detection Module
APD
Multichannel Multi-Tau Correlator
9
APD
SM Fibers
3 cm
Skull
Source
Long Coherence Laser
Activation
1 cm
Cortex

FIG. 8

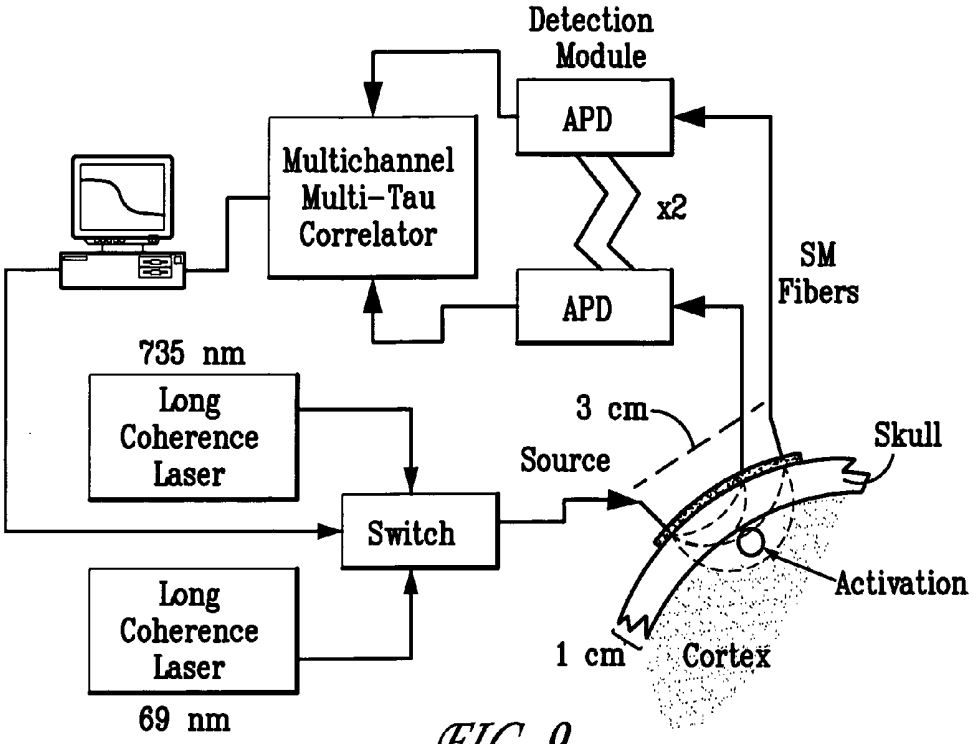
Detection Module
APD
Multichannel Multi-Tau Correlator
x2
SM Fibers
APD
735 nm
Long Coherence Laser
3 cm
Skull
Source
Switch
Activation
Long Coherence Laser
1 cm
Cortex
69 nm

FIG. 9

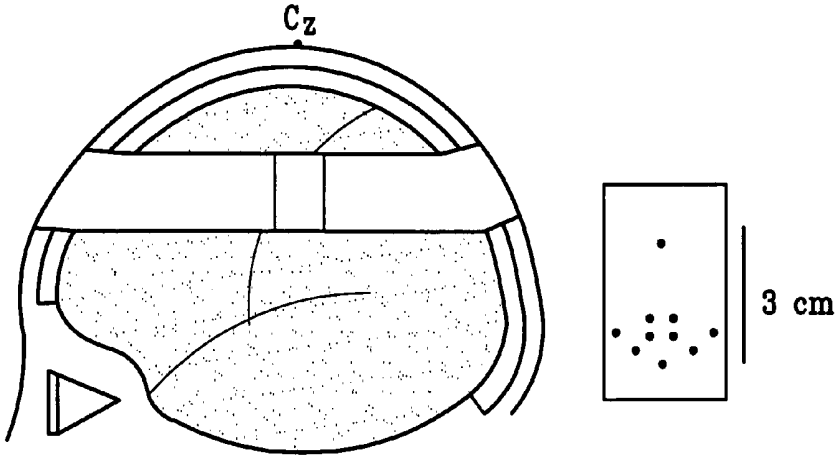
Cz
3 cm

FIG. 10

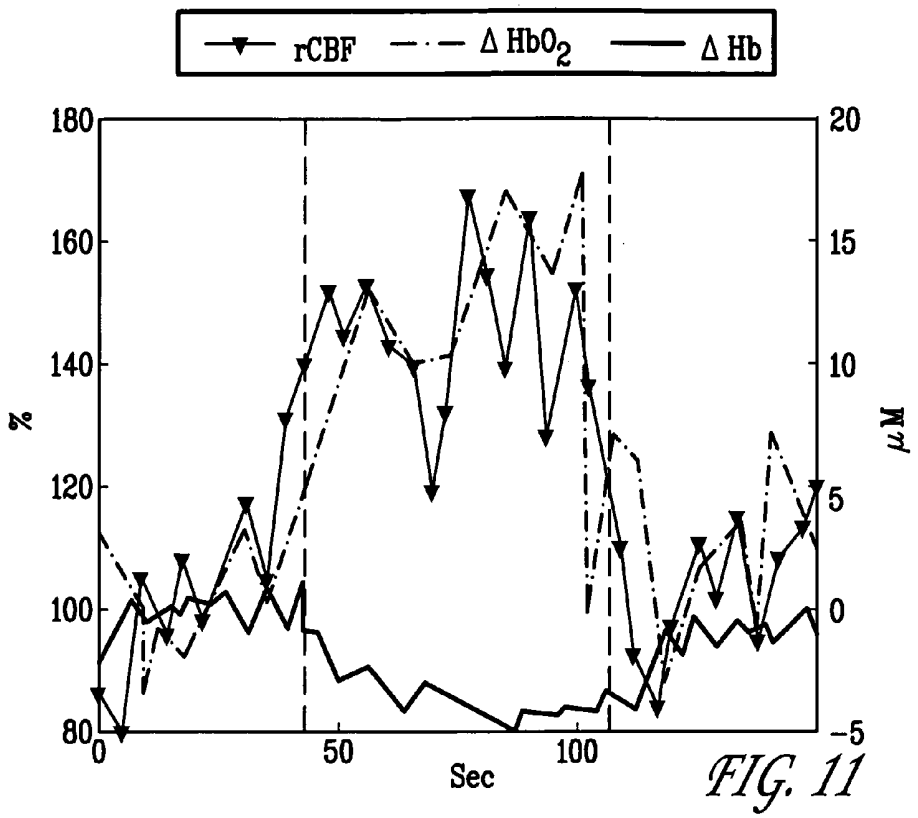
rCBF
Δ HbO2
Δ Hb
180
160
140
120
100
80
%
20
15
10
5
0
−5
μM
0
50
100
Sec

FIG. 11

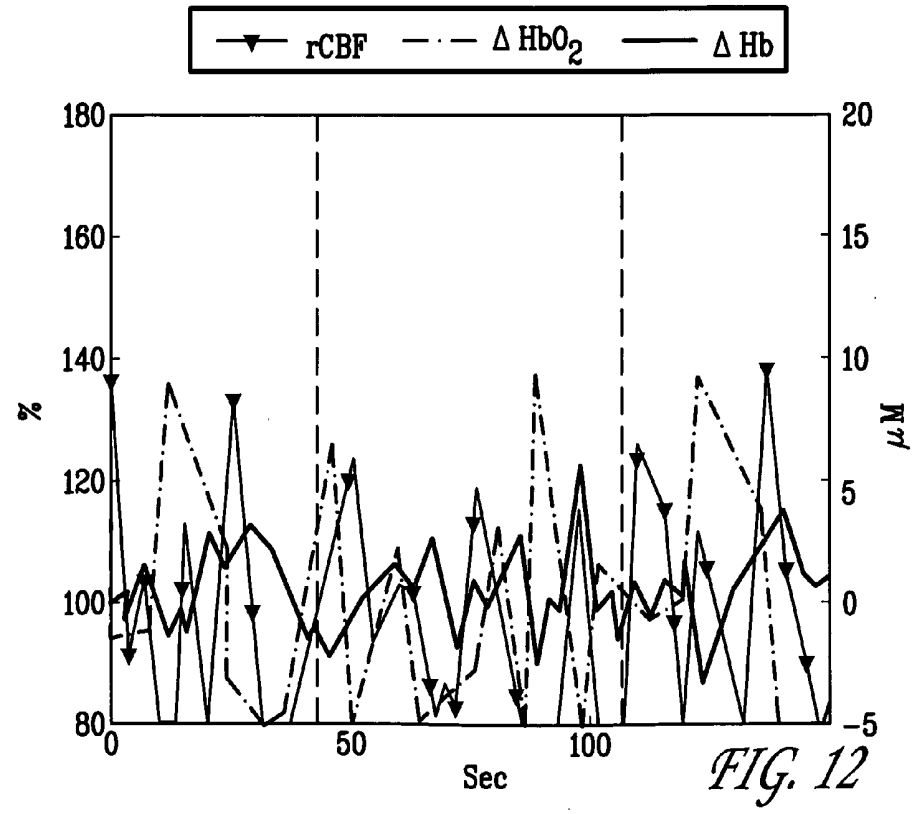
rCBF
Δ HbO2
Δ Hb
180
160
140
120
100
80
%
20
15
10
5
0
−5
μM
0
50
100
Sec

FIG. 12

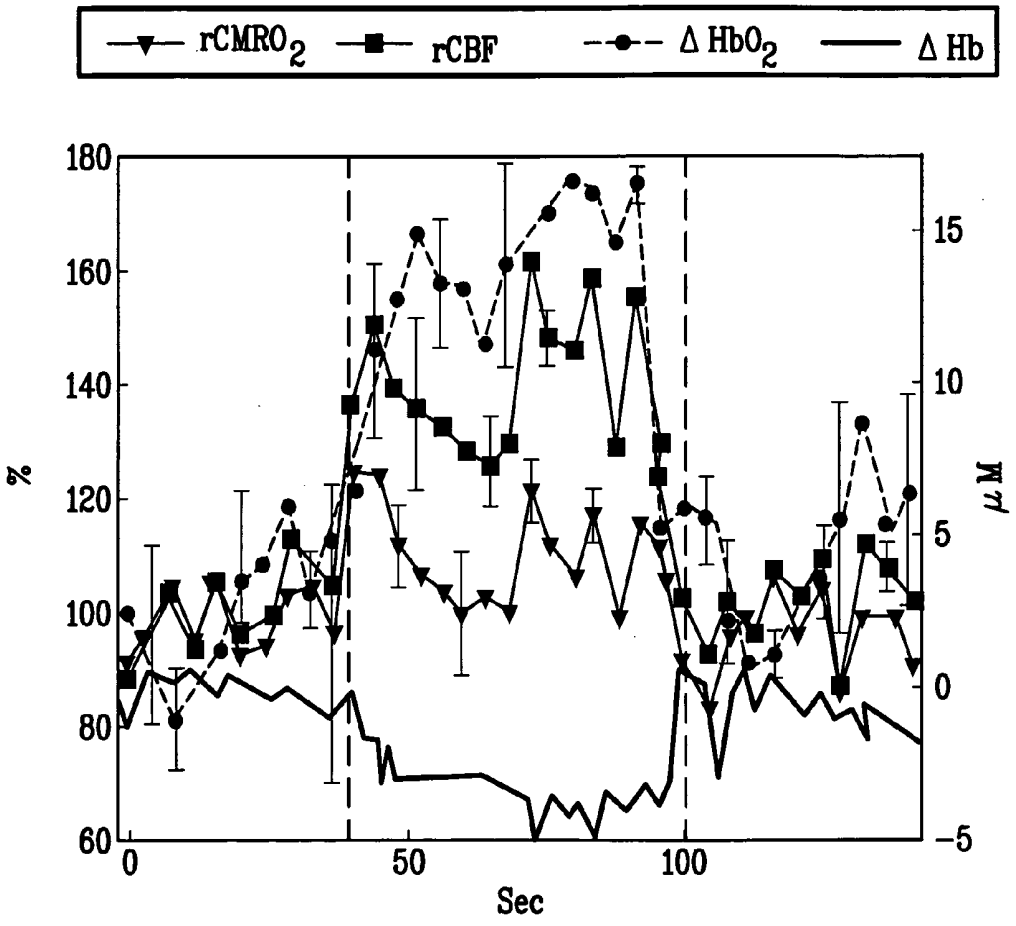
rCMRO2
rCBF
Δ HbO2
Δ Hb
180
160
140
120
100
80
60
%
15
10
5
0
−5
μM
0
50
100
Sec

FIG. 13

OPTICAL MEASUREMENT OF TISSUE BLOOD FLOW, HEMODYNAMICS AND OXYGENATION

FIELD OF THE INVENTION

[0001] The invention relates generally to the measurement of blood flow, oxy- and/deoxy hemoglobins, and oxygenation, scattering and hemodynamic characteristics in tissue. More specifically, the invention relates to methods and apparatus for measuring the flow of blood and oxygenation characteristics using diffuse optical spectroscopy and imaging and diffuse correlation methods.

BACKGROUND OF THE INVENTION

[0002] In the late 1970s, dynamic light scattering theory was applied to living tissue to measure blood flow. Multiple scattering from the blood occurred, resulting for example, in a Doppler broadening of the indirect laser linewidth. In the early 1980s, a theory for how to use diffuse light to measure motional fluctuations in turbid media was discovered. The theory was termed "diffusing wave spectroscopy."

[0003] Diffusing wave spectroscopy enabled a range of dynamical studies of optically dense systems in which scattering particles are moving. However, in these systems, the medium generally was homogeneous in that there were no spatial variations in the dynamic or optical properties. Therefore, these techniques for measuring motions with diffuse light were limited because they could not characterize media with spatially varying, dynamic properties.

[0004] Overtime diffuse imaging and spectroscopy techniques evolved to permit measurement and imaging heterogeneous media such as tissue. The method could be applied to tumors, burns, and other real world structures found in the human body. Such techniques are discussed in detail in U.S. Pat. No. 6,076,010, which is herein incorporated by reference in its entirety. Specifically, these techniques irradiate the medium with a source of light that diffuses through the medium. A measurement is taken of the temporal intensity fluctuations of photon streams that have been scattered within the medium. The medium's properties, for example blood flow rate, are then determined using measured temporal correlation functions of the diffuse light (for example as a function of placement on the tissue surface). We will refer to the methodology as diffuse correlation spectroscopy (DCS).

[0005] Various other methods for measuring blood flow have been developed and employed. For example, conventional venous occlusion plethysmography has been employed for more than fifty years in muscle perfusion investigations. However, this method does not provide regional information and can be used only in the static state, during functional activation, or during brief exercise because it interrupts blood flow. Also, ultrasound Doppler techniques are a common clinical tool used to measure blood flow in large vessels. However, the Doppler techniques are not very sensitive to blood flow in smaller vessels, and do not readily permit continuous measurements during exercise. Laser Doppler techniques also have been used more recently, but typically they only measure the tissue surface. Magnetic resonance imaging (MRI) has high temporal and spatial resolution, and has become a gold standard technique for noninvasive measurement of blood flow and metabolic response. However, MRI's clinical use is limited due to high cost and poor mobility, and it's function form has poor sensitiviy.

[0006] Diffuse correlation spectroscopy (DCS) is an emerging technique for continuous measurement of relative blood flow non-invasively in deep tissues. It has been successfully applied in studies of brain hemodynamics, PDT dosimetry and for measurement of burn depth. DCS enables measurements of relative blood flow (rBF) with high temporal and low spatial resolution in tissue. To date most (but not all) applications of DCS have been in small animal studies wherein source-detector separations were comparatively small. Discussion of DCS techniques has been described in U.S. Pat. No. 6,076,010, which is incorporated herein by reference in its entirety.

[0007] Combining these blood flow rate determinations with oxygenation and hemodynamic tissue properties determined by diffused optical spectroscopy or characteristics further facilitates the understanding of vascular conditions and tissue metabolism, as well as for example in peripheral arterial disease (PAD). In general these improved measurements will enable improved screening of tissues and treatment assessment, as well as to improved fundamental understanding of tissue function. Therefore, there is a real value in such non-invasive optical techniques for study of blood flow, hemodynamics and oxygenation in tissue.

SUMMARY OF THE INVENTION

[0008] An embodiment of the invention includes a device, system and method for determining the characteristics of deep tissue. The novel method includes measuring blood flow rate, hemodynamics and oxygenation characteristics of the tissue, and for determining oxygen metabolism or changes thereof of the tissue. The blow flow rate characteristics are measured by monitoring light fluctuations caused by motions within the tissue, (e.g. blood flow) while the hemodynamics and blood oxygenation characteristics are measured by the transmission of light through the tissue, e.g. with respect to the wavelength of light. The tissue may be layered tissue, for example, a portion of a brain. The tissue characteristics may be measured during times of varying levels of exercise intensity. Also, the invented method may conduct measurement of the autocorrelation function of the transmitted light. The inventive method further may comprise determining an extent of the movement of a blood cell in the tissue, and/or determining the velocity of the movement of a blood cell in the tissue. Also, the blood flow rate, hemodynamics and oxygenation are measured substantially simultaneously. The inventive method may be used to monitor peripheral vascular disease, tumor response, brain activation and/or to determine the efficacy of a drug used to facilitate blood flow.

BRIEF DESCRIPTION OF THE DRAWINGS

[0009] **FIG. 1** is a block diagram of a system for imaging turbid media with spatially varying dynamic properties or spatially varying optical properties provided in accordance with the present invention;

[0010] **FIG. 2** provides a schematic diagram of the hybrid instrument combining diffuse correlation spectroscopy (DCS) and diffuse reflection spectroscopy (DRS) for measuring of bloodflow and oxygenation, according to the invention;

[0011] **FIG. 3** provides a characterization of the flow response during cuff-occlusion, according to the invention;

[0012] **FIG. 4** provides a time curve of relative blood flow and tissue oxygen saturation during arterial occlusion from different source-detector pairs measured on a healthy leg, according to the invention;

[0013] **FIG. 5** illustrates hemodynamic responses during one-minute plantar flexion exercise from a healthy individual and a PAD patient, according to the invention;

[0014] **FIG. 6** provides a time curve of relative blood flow during one-minute plantar flexion exercise from a healthy individual, according to the invention;

[0015] **FIG. 7** provides a schematic of a multi-layer tissue model and the simplified presentation of diffuse light penetration in relation to the different source-detector separations, according to the invention;

[0016] **FIG. 8** provides a block diagram of a basic DCS detection module, according to the invention;

[0017] **FIG. 9** provides a block diagram of another DCS detection module, according to the invention;

[0018] **FIG. 10** illustrates placement of a device on a patient's head, according to the invention;

[0019] **FIG. 11** shows a corrected hemoglobin concentration and flow changes, according to the invention;

[0020] **FIG. 12** shows another corrected hemoglobin concentration and flow changes, according to the invention; and

[0021] **FIG. 13** shows another corrected hemoglobin concentration and flow changes, according to the invention.

DETAILED DESCRIPTION OF ILLUSTRATIVE EMBODIMENTS

[0022] Referring now to the drawings wherein like reference numerals refer to like elements, **FIG. 1** is a block diagram of a system provided in accordance with the present invention for imaging media having spatially varying dynamic properties or spatially varying optical properties.

[0023] A turbid medium is shown generally at **10**, and comprises a substantially heterogeneous matrix **20** wherein there is embedded an object **30**. The object **30** contains small particles which are moving in a non-ordered fashion. "Non-ordered fashion" means that the particles exhibit Brownian motion, turbulent motion, shear flow, random motion, velocity changes or any other motion which results in a change in the relative distance between the particles. This is what is meant by the term "dynamic" throughout. In practice the background medium could also be "dynamic." In an experimental setup which has been used to verify the systems of the present invention, the matrix **20** is a solid slab of titanium dioxide suspended in resin, and the object **30** is a small cavity with a 0.2 percent suspension of 0.296 micrometer diameter polystyrene spheres. The slab has dimensions of 15.times. 15.times. 8 centimeters.

[0024] A source of light **40** is coupled by a multimode fiber **50** to the medium **10**. Preferably, the source **40** is a coherent source of energy. Even more preferably, the source is a laser or a stable light source, well known to those skilled in the art. Most preferably, the source is an argon ion laser which outputs energy in the 514 nanometer green wavelength range.

[0025] A fiber **60** is placed at a known position with respect to the matrix **20**, and will pick up light which diffuses through the medium **10**. A detector **70** is interfaced to the fiber, and by standard gain techniques creates a signal which is representative of the intensity fluctuations at the fiber resulting from the photons which have diffused through the medium **10** and which may have scattered from the particles in object **30**. Any detector which can produce a gain, for example a photomultiplier tube, can be interfaced with the fiber **60**, and it will be recognized by those with skill in the art that a fiber-detector combination will produce the results required in accordance with the invention. A preferred embodiment of fiber **60** is a single mode fiber.

[0026] In accordance with the present invention, a digital autocorrelator **90** is interfaced with the photomultiplier tube **70** in order to observe the intensity fluctuations of the signal speckle. The digital autocorrelation device **90**, which is a well-known electronic system that is commercially available, measures the temporal intensity autocorrelation function of the photons received by the detector. As will be described in more detail below, this autocorrelation function can be used to obtain the scattering, absorption and dynamic characteristics of the medium in accordance with the methodology described herein.

[0027] In accordance with the invention, autocdrrelation functions are measured with the source and collecting fibers individually positioned at different locations with respect to the object **30**. A computer processor **100** with the appropriate software that implements the correlation diffusion theory described below determines the scattering, absorption and dynamic characteristics of the medium from the diffusion correlation wave and thereby reconstructs an image of the dynamically heterogeneous medium **10**. Also, the computer may include software that allows a calculation of a correlation function. The computer can be any known, standard processor which can utilize the correlation information output by the autocorrelator **90**. In this manner, a reconstructed image of the medium **10** having the object **30** therein can be produced as a function of the scattering and absorption of the diffuse correlation wave as it propagates diffusing through the medium **10**.

[0028] It has been demonstrated that transmission and remission measurements of diffuse light intensity emerging from heterogeneous turbid media can provide adequate information for the construction of low resolution images of the spatially varying absorption and scattering coefficients. When the medium is dynamic, the time-dependent density fluctuations of the sample are impressed upon the temporal behavior of the diffusing light. For homogeneous fluctuating turbid media, the temporal intensity autocorrelation function of an emerging speckle of diffuse light can be analyzed to provide information about the temporal fluctuations within the sample. This is the technique we will refer to as diffuse correlation spectroscopy. Just as diffuse photon density waves can be used to probe the spatial variations in absorption and scattering coefficients within heterogeneous media, position-dependent measurements of the temporal autocorrelation function of diffusing light fields can be used to generate images of temporal fluctuations within heteroge-

neous turbid media. The techniques of the present invention provide a new contrast mechanism for imaging within turbid media. Specifically, these techniques can distinguish regions of strong and weak density fluctuations such as calcium deposits versus soft tissue or blood flow versus stasis.

[0029] **FIG. 2** provides a schematic diagram of a hybrid measurement instrument. The hybrid instrument may employ lasers having two or more wavelengths (e.g., in this case 676 nm, 786 nm, 830 nm) that are modulated at 70 MHz to perform diffuse reflection spectroscopy (DRS). A continuous wave laser with a relatively long coherence length (e.g. at 800 nm) may be used for diffuse correlation spectroscopy (DCS). As illustrated in **FIG. 2**, the probe may include any number of possible configurations including a DCS source (cross) fiber located at the center of eight DCS detector fibers. Also, the probe may include four DRS detector fibers and six DRS source fibers (empty circle) arranged on a 3 cm radius circle. It should be appreciated that a flexible material (e.g., silicone) may be used to tightly hold the fibers in place, and elastic straps may be used to maintain the probe in proximity to the muscle.

[0030] Source-detector separation may range, for example, from 0.5-3 cm for DCS and 0.5-6 cm for DRS. The sampling time for DCS measurement may be approximately 1.5 seconds. A complete frame of data, cycling through all source-detector pairs, was acquired in 2.5 seconds. Also, the probe may employ computer devices to control the DRS and DCS.

[0031] Generally, the measurement techniques derive tissue optical properties, for example, hemoglobin concentration and blood oxygen saturation from diffuse reflection spectroscopy (DRS) measurements, and blood flow from diffuse correlation spectroscopy (DCS) measurements.

[0032] First, DRS for blood oxygenation, the tissue is modeled as a semi-infinite homogeneous medium. A wavelength-dependent semi-infinite analytical solution to the photon diffusion equation can be used to fit for the optical properties of the underlying tissue. Other models, numerical and analytical based on the diffusion equation are used to analyze more heterogeneous (e.g., largest tissues). The properties of the tissue may be characterized by a number of techniques. For example, the optical properties of the tissue may be characterized by an absorption coefficient $\mu_\alpha$and a reduced scattering coefficient μ_s'.

[0033] The multi-distance and multi-wavelength DRS measurements of diffusive waves on the tissue surface provide information about tissue absorption ($\mu_\alpha$has been dubbed "diffusing wave"). The wavelength-dependent optical absorption coefficient may then be decomposed into contributions from different tissue chromophores, i.e., $\mu_\alpha(\lambda)=\Sigma_i\epsilon_i(\lambda)c_i$. The sum is over all relevant tissue chromophores; $\epsilon_i(\lambda)$ is the extinction coefficient as a function of wavelength for the i^{th} chromophore, and c_i is the concentration of the i^{th} chromophore. The c_i are unknowns to be reconstructed from the wavelength-dependent absorption information. Oxy- and deoxy-hemoglobin concentrations (e.g., CHb, $CHbO_2$ respectively) along with water lipid concentration typically are the largest tissue absorbers in the NIR. Combinations of these parameters yield tissue total hemoglobin concentration (THC=CHb+$CHbO_2$) and tissue blood oxygen saturation (S_tO_2=[$CHbO_2$/(CHb+$CHbO_2$)]× 100), as well as tissue slattering.

[0034] Next, DCS for relative blood flow, consider speckle fluctuations of the diffuse light that are sensitive to the motions of tissue "scatterers," for example red blood cells. The quantity containing this information is the electric field (E(r,t)), and the electric field temporal autocorrelation function. $G_1(r,t)=<E(r,t)\,E^*(r,t+\tau)>$, or its Fourier Transform is related to the motion of the red blood cells. Here the angle brackets < > denote averages over time and τ is called the correlation time.

[0035] The study of motions in deep tissues is available because the electric field temporal autocorrelation function for light traveling in highly scattering media obeys typical correlation diffusion equation techniques. The correlation diffusion equation can have different forms depending on the nature of the particle motion, and on the variations of these motions with respect to position in the sample. For example, for the random flow that can arise in the tissue vasculature, the mean-square displacement, ($<\Delta r^2(\tau)>$), of the scattering particles (e.g., blood cells) in time τ is $(\Delta r^2(\tau)>=V^2)\tau^2$. Here, ($V^2$) is the second moment of the cell speed distribution. In this case the correlation function $G_1(r,\tau)$ will decay approximately exponentially in τ. Its decay rate, $\Gamma(sec^{-1})$, depends on a parameter α (proportional to the tissue blood volume fraction), and on the motion of blood cells. Relative changes in $\Gamma(sec^{-1})$ correspond to relative changes in blood flow.

[0036] For blood oxygenation and flow in different layers the investigated tissue is layered (e.g., skin, adipose tissue and muscle or skull and cortex). Based on diffusion theory, the most probable penetration depth of diffuse light in tissue is roughly one-half to one-third the separation of source detector pairs on the tissue surface. In other words, the blood oxygenation and hemoglobin characteristics are derived based on the positioning of the source detector. Therefore, specific source-detector separation pairs provide information about particular tissue layers. Relative blood flow (rBF) in specific layers may be obtained using the DCS data derived from a corresponding single source-detector pair with appropriate separation. Similarly, DRS data from the same source-detector pair may be normalized with its baseline value to calculate the relative change of tissue blood oxygen saturation (ΔS_tO_2) for the corresponding layer. Also, absolute baseline S_tO_2 may be estimated from multi-distance DRS measurement. Multi-distance DRS and DRS measurements may also be used to derive images of these quantities based on diffusion equation analysis.

[0037] In the calculating blood oxygenation and flow, nominal influence on calculation accuracy was determined by the assumed baseline value of the scattering coefficient μ_s'. Furthermore, even this nominal error may be avoided by employing additional source fibers and by calibrating the coupling coefficients of the instrument more accurately.

[0038] Tissue metabolic rate of oxygen consumption ($TMRO_2$) may be modeled in a similar manner as is done with the cerebral metabolic rate of oxygen consumption ($CMRO_2$). In particular, $TMRO_2$ may be calculated by combining the blood flow data and oxygen saturation data. In steady-state, $TMRO_2$ depends on the difference in oxygen concentration across the vasculature (i.e., arteriole minus venous) multiplied by the blood flow rate, or $TMRO_2$= (OEF)×(BF)×($[O_2]a$), an equation sometimes referred to as Fick's Law, where $[O_2]_a$ is the arterial oxygen concentration, OEF is the oxygen extraction fraction defined as ($[O_2]_a$–

$[O_2]_v)/([O_2]_a)$, and where subscripts v and a denote venous and arterial sides, and where BF is tissue blood flow. This is a general equation typically used in analysis of oxygen metabolism problems, particularly those associated with activation in brain and muscle. It could be replaced with any other adequate model.

[0039] Assuming the arterial oxygen concentration, $[O_2]_a$, does not change, the relative change in oxygen metabolism can be shown to be: $rTMRO_2=rOEF \times rBF$, where r denotes relative change, and where differential changes in the temporal decay of diffuse photon correlation functions yield rBF. Also, the oxygen extraction fraction, OEF, is further related to tissue blood oxygen saturation. Therefore, the DCS measurement allows for a determination of relative blood flow, rBF, and the DRS measurements enables a determination of rOEF, where $OEF=(S_aO_2-S_tO_2)/(\gamma x S_aO_2)$ where S_aO_2, and S_tO_2 are arterial and tissue saturations respectively, and γ indicates percentage of blood volume contained in the venous component of the vascular system. OEF can be obtained direct from the measured S_tO^2. Also, if γ remains constant, then the compartment parameter divides out of the measure of rOEF.

[0040] The measured responses permit derivation of time curves for tissue oxygen saturation (% S_tO_2), total hemoglobin concentration (THC (μM)) and relative blood flow (rBF (%)). For example, a time curve for relative tissue metabolic rate of oxygen consumption ($rTMRO_2$ (%)) may be determined for plantar flexion exercise used in exercise rehabilitation and therapy. $TMRO_2$ does not substantially change ($rTMRO_2=1$) throughout the arterial occlusion because there is no functional activity during ischemia. Therefore, a linear regression of the oxygen desaturation rate occurring during the first 60 seconds of ischemia can be used for calculating the $TMRO_2$ level at rest.

[0041] To characterize hemodynamic responses, mean and standard deviation are tabulated for maximal change (Max Δ), wave time constants from manipulation onset (T_m (sec)) to maximal response, recovery half-times (T_{50} (sec)) and amount of overshoot (OS (Δ)). **FIG. 3** shows an example for characterization of the blood flow response (rBF) during a cuff occlusion. Other variables (e.g., S_tO_2, THC and $rTMRO_2$) during cuff occlusion and exercise may be characterized in the same manner.

[0042] **FIG. 4** shows the rBF (top) and S_tC_2 (bottom) responses during leg arterial occlusion from different source-detector pairs measured on a healthy individual. The source-detector separations, may be any length, for example, 0.5, 1.5, 3, 4, and 5 cm for DRS, and 0.5, 1, 2, and 3 cm for DCS respectively. **FIG. 4** indicates that stronger reactive hyperemia (peak flow overshoot) after the release of occlusion, and deoxygenation during occlusion were derived from the separations of 2 cm for DCS and 1.5 cm to 5 cm for DRS, respectively. Similar responses of the different layers were also found in arm cuff occlusion. The stronger responses are mainly from the muscle layer, and separations with the stronger response are used to analyze the data.

[0043] Table 1 lists the hemodynamic responses in cuff occlusions from ten healthy volunteers and one PAD patient. % S_tO_2 and THC (uM) were fitted using data derived from source-detector separations of 1.5-5 cm and rBF (%) was calculated by averaging signals from the two 2 cm source-detector separations in different locations.

TABLE 1

Responses in cuff occlusions from ten healthy volunteers and one PAD patient.

Parameters	Subjects	T_m (sec)	Max Δ	T_{50} (sec)	OS (Δ)
		Leg occlusion			
StO2	Healthy	177.1 ± 20.7	−16.4 ± 4.4	33.7 ± 26.0	3.8 ± 1.7
(%)	PAD	180.0	−15.0	96.0*	3.0
THC	Healthy	88.1 ± 81.9	−1.8 ± 5.9	16.2 ± 18.3	2.8 ± 3.1
(μM)	PAD	25.0	−10.0	36.0	5.0
rBF	Healthy	51.0 ± 11.5	−90.0 ± 2.4	25.6 ± 14.5	311.4 ± 90.8
(%)	PAD	60.0	−93.0	90.0*	165.0*
		Arm occlusion			
StO2	Healthy	174.7 ± 15.3	−25.1 ± 8.2	19.4 ± 15.2	11.4 ± 5.0
(%)	PAD	180.0	−23.0	23.0	10.0
THC	Healthy	46.6 ± 61.2	−1.4 ± 6.4	13.6 ± 7.3	8.6 ± 5.0
(μM)	PAD	111.0	−16.0	20.0	22.0
rBF	Healthy	14.0 ± 7.4	−90.3 ± 3.8	11.3 ± 6.1	445.1 ± 194.1
(%)	PAD	11.0	−92.0	12.0	450.0

[0044] As noted from Table 1, for healthy volunteers, cuff occlusion of the leg flexor and arm flexor muscles produced a similar response. In particular, the rapid increase of cuff pressure induced a rapid and substantial decrease in rBF: Max $\Delta rBF=-90.0\pm2.4\%$ for leg and Max $\Delta rBF=-90.3\pm3.8\%$ for arm, assigning a baseline value of 100%. Also, a gradual decrease in S_tO_2 occurred throughout the arterial occlusion. The minimum measurable blood flow (~10% of the baseline value) during cuff occlusion is the so-called "biological zero." Also, rBF reached this "biological zero" within the first minute whereas S_tO_2 started to decrease rapidly, but did not reach a minimum for approximately 5 minutes.

[0045] During cuff occlusion, total hemoglobin concentration (THC) was generally unchanged, however, there was a variation between trials. Also, it was noted that the hemodynamic response trends in the PAD patient are similar to those of the healthy volunteers, and no substantially different responses were found in arm muscle between patient and healthy controls. However, as noted in Table 1, in the patient leg muscle, the relative magnitude of reactive

hyperemia was approximately ½ of the controls, and the recovery halftimes of both S_tO_2 and rBF after occlusion were about triple the controls.

[0046] **FIG. 5** illustrates the typical time curves of S_tO_2 and THC (shown on the top), and rBF and $TMRO_2$ (shown on the bottom) during plantar flexion exercise from a healthy individual (shown on the left) and a PAD patient (shown on the right). rBF during exercise did not show different phases of the muscle activity (contraction and relaxation) due to the comparatively long sampling time (2.5 seconds). In a separate trial with higher temporal resolution (i.e., approximately 1 Hz) achieved by changing the measurement duration for DCS (in expense of lower signal-to-noise ratio) and using only one source position for DRS measurement, flow oscillations that correlated with the muscle contraction and relaxation were exhibited.

[0047] Table 2 summarizes the mean ± standard deviation from ten healthy volunteers and one PAD patient.

Parameters	Subjects	T_m (sec)	Max Δ	T_{50} (sec)	OS (Δ)
StO2	Healthy	29.4 ± 8.7	−17.1 ± 7.9	36.7 ± 22.8	4.8 ± 3.6
(%)	PAD	22.0	−12.3	70.0*	3.0
THC	Healthy	18.3 ± 9.6	−17.6 ± 9.9	23.7 ± 13.9	3.3 ± 3.9
(μM)	PAD	12.0	−32.8*	16.0	10.0
rBF	Healthy	14.9 ± 8.1	473.7 ± 138.6	NA	−9.5 ± 19.5
(%)	PAD	12.0	240.0*	NA	−10.0
$rTMRO_2$	Healthy	14.9 ± 8.1	694.5 ± 176.5	NA	−7.5 ± 15.9
(%)	PAD	12.0	338.4*	NA	0.0

[0048] The healthy muscle responses showed variations among subjects. Within a short time (14.9±8.1 seconds) after the exercise began, $rTMRO_2$ increased approximately 7 fold (694.5±176.5% assigning a baseline value of 100%). To meet the increase in oxygen demand, rBF increased rapidly and reached a maximum (473.7±176.5%, assigning a baseline value of 100%) in the same short time (14.9±8.1 seconds). This increase in flow during exercise is termed active hyperemia.

[0049] The greatest discrepancy between rBF and $rTMRO_2$ occurred in approximately 15 seconds demonstrating the maximum mismatch between oxygen delivery and oxygen demand. THC decreased and reached a minimum (Max ΔTHC=−17.6±9.9 μM) almost as fast as rBF, while S_tO_2 started to decrease rapidly and reached a minimum (Max ΔStO_2=−17.1±7.9%) in 29.4±8.7 seconds. After reaching the maximum or minimum, those variables fluctuated around their extremes.

[0050] Once exercise ceased, rBF and $rTMRO_2$ recovered to their baselines rapidly whereas THC and S_tC_2 increased more slowly towards their baselines. The recovery half-time (T_{50}) of rBF and $rTMRO_2$ after occlusion were so fast that they were not measurable with the present temporal resolution (i.e., 2.5 second sampling time) of the instrument.

[0051] A similar variation was observed between left/right arm/leg of healthy individuals. The PAD patient and the healthy volunteers had similar dynamic response trends to the plantar flexion exercise. The differences between the PAD patient and the healthy volunteers were primarily in magnitude of the active hyperemia (rBF), total hemoglobin concentration (THC) and oxygen consumption rate ($rTMRO_2$) during exercise, and the recovery half-time of S_tC_2 after exercise in the leg muscle. The relative magnitudes of active hyperemia, THC and $rTMRO_2$ during exercise were half of the controls, and the recovery half-time of S_tC_2 after exercise were double the controls.

[0052] **FIG. 7** displays a multi-layer tissue model and a schematic of diffuse light penetration for the different source-detector separations. In particular, **FIG. 7** simulates the configuration of the DCS blood flow measurements in leg. As shown in **FIG. 7**, the signal detected by the source-detector pair with separation of 2 cm derives mainly from the muscle layer, whereas signals from shorter separations are from upper layers. An accurate quantification of the penetration depth of diffuse light requires consideration of the tissue optical properties and the thickness of each layer, as well as a multi-layer model are necessary. Penetration depth may be estimated by experimentally calibrating using the reactive hyperemia measurement after arterial occlusion release.

[0053] Reactive hyperemia, following rapid release of arterial occlusion, is a transient increase in blood flow. The ability of an organ to display reactive hyperemia is related to its ability to display auto-regulation. Different organs display varying degrees of auto-regulatory behavior. For example, skeletal muscle shows moderate auto-regulation, while the cutaneous microcirculation shows little or no auto-regulatory capacity. The reactive hyperemia occurs because during the period of occlusion, tissue hypoxia and a build-up of vasodilator metabolites (presumably dilate arterioles) decrease vascular resistance. When compared with muscle tissue, both oxygen consumption and oxygen extraction are much lower in adipose tissue. Therefore, the lower metabolism accumulates less vasodilator metabolites during arterial occlusion in adipose tissue, inducing lower magnitude of reactive hyperemia.

[0054] From **FIG. 4** it is noted that the magnitude of reactive hyperemia derived from the source detector separation of 2 cm is more than 2 times greater than those from shorter separations. Taken together, the result derived from the simulation (in **FIG. 6**) and the measurement (see **FIG. 4**), suggest that the strongest hyperemia signal (2 cm separation) is derived from the muscle tissue layer, while the weaker responses are due to the source-detector pairs with shorter separations and represent the response of cutaneous tissues.

[0055] Similarly, decreases of S_tC_2 during arterial occlusion derived from the separation of 1.5 cm to 5 cm are much

higher than those from 0.5 cm separation (in **FIG. 4**), and thus represent response of the muscle layer. These findings suggest that both DRS and DCS can probe through the upper tissue layers into the muscle, based on the choice of source-detector separations in the appropriate range for these measurements.

[**0056**] The hemodynamic responses of healthy muscle tissues have demonstrated comparable and repeatable variations during hemodynamic perturbations. At the onset of the arterial occlusion, blood flow rapidly goes to "biological zero." S_tO_2 on the other hand, decreases gradually during the occlusion because of continuous oxygen consumption in tissues and minimal blood flow (oxygen delivery). The declining rate of muscle oxygenation reflects the level of tissue oxygen consumption rate at rest. When the occlusion is released, there is a reactive hyperemia because of the auto-regulation (vasodilation) of muscle vasculature in response to metabolites created during ischemia.

[**0057**] During the hyperemia, oxygen is replenished and the metabolic stimulus for vasodilation is washed out, causing vasoconstriction. Thus blood flow and oxygen return to their normal resting levels respectively. The reactive hyperemia has important physiological implications because it is related to the ability of muscle vasculature to auto-regulate.

[**0058**] Characterization of dynamic exercise is more difficult because of its complexity and the speed of metabolic mechanisms. Exercise consumes large amounts of energy and therefore requires delivery of considerable amounts of oxygen and substrate (e.g., glucose, protein, ion), as well as the removal of waste metabolites (e.g., CO_2, H^+, lactate). The intrinsic auto-regulation ability in muscle vasculature increases blood flow to meet the increased need for delivery and removal. This increase in flow is termed "active hyperemia" and is often brought about by the reduction of vascular resistance (vasodilation).

[**0059**] Tissue hypoxia and accumulated vasodilator metabolites during exercise dilate arterioles and thus decrease vascular resistance. Moreover, the "skeletal muscle pump" and "vascular recruitment" also facilitate blood flow during muscle exercise. Mean blood flow increases during plantar flexion exercise (in **FIG. 5**). However, if blood flow is measured without averaging, the flow will be seen in two phases—i.e.,—decrease flow during contraction and increase flow during relaxation.

[**0060**] Using a higher temporal resolution (e.g., approximately 1 Hz), diffuse correlation spectroscopy (DCS) can capture these two phases (in **FIG. 6**). The increased blood volume during muscle relaxation mainly increases blood in the capillary component as previously "unused" capillaries open (i.e., vascular recruitment). In contrast, the muscle contraction mainly compresses the vascular tree in the venous component propelling blood towards the heart (skeletal muscle pump).

[**0061**] The magnitude of the active hyperemia (i.e., rBF) is closely related to the increase in tissue metabolic rate ($rTMRO_2$) throughout the period of exercise. However, the average increases were quite different (**FIG. 5** and Table 3). Also, the average increase in blood flow at the transition from rest to the exercise was approximately 4.7 fold whereas the average increase in $rTMRO_2$ was approximately 7 fold. The increase in rBF was significantly lower than the increase in $rTMRO_2$ ($p=0.006$, two-sample t-test). Therefore, a gradual decrease in tissue oxygenation saturation (S_tC_2) was produced, indicating that increased oxygen demand may not be completely met by an increase in blood flow.

[**0062**] The ability to evaluate how muscle blood flow responds to energy demands is a useful assessment tool. For example, the mismatch between blood supply and oxygen demand is considered to be an important factor in determining the cellular depletion of energetic metabolites, and the magnitude of active hyperemia during exercise is believed to be related to the vascular response to these metabolites.

[**0063**] The different responses between healthy volunteers and the PAD patient are illustrated in Table 1 and Table 2. As shown in Tables 1 and 2, the relatively longer recovery half-times of S_tC_2 (T_{50}=96 seconds for cuff occlusion and T_{50}=70 seconds for exercise) were found in a diseased leg. Also, a longer recovery half-time of rBF (T_{50}=90 seconds) was also found in the diseased leg after release of the cuff occlusion. In addition, as shown in Table 2, the magnitude of active hyperemia (rBF) and $rTMRO_2$ during the exercise in the diseased leg were only half of those in healthy volunteers.

[**0064**] As shown in Table 1, a similar observation was found in the magnitude of reactive hyperemia during the arterial occlusion in the diseased leg. These weaker flow (dilation) responses may help determine the affecting the oxygen delivery and ability to support muscle metabolism. As shown in Table 2, less blood flow delivery during exercise in the diseased leg leads to a greater decrease of tissue total hemoglobin concentration (THC).

[**0065**] In sum, the novel techniques permit DCS to penetrate through layers of upper tissues to muscle tissue. As a result, this technique provides more accurate measurement of blood flow in muscle capillary bed compared than currently available. This is because the technique is not adversely affected by the blood flow from the surrounding tissues (e.g., cutaneous tissues, bone, tendons). The DCS technique does not interrupt the blood flow during measurement. Also, because of the ease of its noninvasive nature, the technique can be used in different dynamic conditions. The efficacy of the novel technique for DCS flow variation is approximately 7.6 times lower than MRI flow variation techniques.

[**0066**] Also, the combination of DCS and DRS techniques has permitted the use of both optical techniques non-invasively and continuously to measure rBF, S_tO_2 and THC in deep muscle tissues under rest as well as during mild exercise and extreme cuff occlusion perturbations. These hemodynamic parameters permit an estimation of the changes of index $rTMRO_2$. Also, these techniques permit portable and relatively inexpensive hybrid instrumentation that may be conducted in a clinical routine examination. Quantification of hemodynamic responses (e.g., reactive hyperemia, active hyperemia, mismatch between blood supply and oxygen demand, recovery half-time) is also useful for estimation of physiological states. Such information may facilitate improved diagnostic and treatment options for patients with PAD.

[**0067**] The novel techniques also facilitate treatment and detection of various other maladies. **FIGS. 8 and 9** provide an illustration of a probe that uses DCS and DRS techniques.

FIG. 8 illustrates a block diagram of a basic DCS detection module and **FIG. 9** provides a diagram of a DCS detection module using two laser devices.

[**0068**] **FIG. 8** provides a block diagram of a basic DCS detection module. The novel apparatus employs high quality single-mode fibers that operate in certain wavelengths (e.g., 800 nm) and that are isolated from light leaks. The detector is a fast, photon counting avalanche photodiode (APD) with low dark current, for example a model SPCM-AQR-14, manufactured by Perkin-Elmer of Canada. The APD may include an amplifier-discriminator unit that outputs a standard TTL signal corresponding to the number of photons counted. This signal may be fed to a fast, multi-Tau correlator board. These boards are software configured and are available in multi-channels.

[**0069**] One curve is obtained by the device every 106 ms. Each individual curve may be outputted or an average of many curves may be outputted. The signal-to-noise ratio increases with the square root of the number of curves averaged. The multi-Tau technique uses a quasi-logarithmic spacing of the temporal bins allowing collection of a large range of delay times with a limited (e.g., 255) channels which is essentially equivalent to using 255 independent correlators with increasing delay times (doubled at each octave).

[**0070**] Correct choice of the bin spacing avoids triangular averaging related errors and is defined by the correlator hardware. The output from the correlators may be combined to obtain the desired autocorrelation function. This method improves the signal-to-noise while keeping a large dynamic range (in delay times) and therefore, the efficiency.

[**0071**] A DCS light source module may be a long coherence laser, for example, a diode pumped laser diode working at continuous wave mode, for example, a 800 nm, model TC40, manufactured by SDL Inc, of San Jose, Calif.). The light at several separations (e.g., 1.5, 2.0, and 3.0 cm) are detected and the temporal autocorrelation functions are calculated by the correlator board. The multi-channel design enables adequate signal-to-noise by averaging some curves (i.e., 1060 ms per data-point).

[**0072**] In addition, a second laser source may be added as shown in **FIG. 9**. The second laser source may be a 690 nm laser manufactured by Crystal Laser and a 2×1 optical switch to share source positions, as shown in **FIG. 4**. Also, the laser source may be connected via an electrical switch so as to share detectors. Using a second laser doubles the data acquisition time (e.g., approximately 2 seconds), and also enables simultaneous measurements of tissue oxygenation. The computer controlled optical switch may be used to share the source fiber between two lasers. This is accomplished by recording the detected, average intensity at each detector position and each wavelength and using continuous wave near-infrared spectroscopical methods, well known to those skilled in the art.

[**0073**] Although not shown it should be appreciated that the device may include various other components well known to those skilled in the art, including but not limited to, CCD camera, photomultiplier, photodiode, avalanche diode, photomultiplier tubes, etc.

[**0074**] A DCS analyzer may be used to analyze blood flow. In particular, as is well known to those skilled in the art, blood flow data is analyzed by fitting each autocorrelation curve to a model, for example, a semi-infinite, many layer diffusion model. The flow measurements yield relative CBF (rCBF). For quantification, the partial volume effects may be reduced by using a two layer model with the top layer (skull) thickness set at 1 cm with a flow less than 1% of the bottom layer (brain). Similarly, the CW intensity data at both wavelengths will be fit to a multi-distance, two-layer diffusion model, yielding the oxy- and deoxyhemoglobin concentrations. Tissue oxygen saturation and total hemoglobin concentration may be calculated from these measurements.

[**0075**] The novel extraction of two different data types enables relative changes in $CMRO_2$ ($rCMRO_2$) to be derived from the measured variation in blood flow, deoxy-hemoglobin concentration, and total hemoglobin concentration. In this model, a constant arteriol-venous tissue compartmentalization may be assumed, and for slow variations (i.e., approximately a few seconds), $rCMRO_2$ is found to be proportional to the product of rCBF and relative changes in deoxy-hemoglobin and total hemoglobin concentration.

[**0076**] One set of applications involves the study, diagnosis, monitoring and treatment of the brain. In particular, DCS probe may be used to study functional activation of the human brain. **FIG. 10** illustrates placement of the device on the patient's head to facilitate such investigation of the brain. Eight DCS detectors may be used, for example, at 2 cm (×2), 2.5 cm (×2) and 3 cm (×4) distance from a source placed at the center of a circle (radius=3 cm). The probe may be fastened using elastic, medical bandages. The fibers may be custom built with special ferrules at the end and are held in place.

[**0077**] In one study, illustrated with respect to **FIGS. 11-13**, a patient was instructed to tap their index and middle fingers against the thumb at 3 Hz, in time with an auditory cuing signal. A 1-min baseline was recorded before and after each stimulus, and a blocked design of 15 such stimuli was used. One patient was asked to repeat the study using the ipsilateral hand to confirm the contralateral nature of the optical response, and with another subject 30 seconds of stimulus were obtained, and signals were compared with those of 1 minute stimulus duration.

[**0078**] **FIG. 11** shows the corrected hemoglobin concentration and flow changes. The graph in **FIG. 11** indicates a sustained rise in oxyhemoglobin, a decrease in deoxyhemoglobin, with an increase in CBF. **FIG. 12** illustrates that if the probe was placed 2 cm frontal to the motor cortex, the effect of the finger tapping was clearly absent, demonstrating the local nature of the response. **FIG. 13** illustrates that the increase in $CMRO_2$ due to finger tapping was 10.1±4.4% within the range of values (9%-29%) from hybrid MRI measurements. The ratio of rCBF to $rCMRO_2$ is 3.8±1.1.

[**0079**] Notably, when the stimulus duration was 30 seconds instead of 60 seconds, the measured amplitude did not change significantly, but the peak duration was halved. No response was visible on the side ipsilateral to the stimulated hand, and measurements when the probe was placed far away from the sensorimotor cortex did not exhibit any significant changes in signal. Therefore, this investigation validates that the efficacy of the hybrid instrument that combines diffuse optical and correlation spectroscopies to measure concurrent variations of blood flow, blood oxygen-

ation, and oxygen metabolism through the intact skull of an adult human brain during sensorimotor cortical activation. Metabolism may be determined using a bulk overall value technique, and may be measured at one or more locations. Blood metabolism may be measured as two dimensional or three dimensional imagers.

[0080] In another application, many sick infants are admitted to the pediatric neuro-intensive care unit (PNICU) with severe cerebral hypoperfusion due to cardiac disease as well as other conditions. The management of these individuals is complicated due to their age and fragility. Yet, infants are more able to benefit from the novel techniques because an infant's skull is thinner and even more transparent than an adult patient. Also, these novel techniques can provide the ability to do extensive research on the nature and progress of disease in comparison to the development of healthy infants. Another application for the novel techniques involves sleep studies of patients with sleep disorders. Patients with symptoms indicating sleep disorders such as sleep apnea are regularly diagnosed through a series of doctor visits with different specialties and tests of varying complexity. The diagnosis of sleep apnea is complicated because many factors can disturb sleep. The novel technique can improve the acquisition of data related to sleep disorders because cerebral blood flow can be monitored regionally and continuously and can be related to the brain metabolic state, without significantly disturbing the patient's normal sleep process.

[0081] The novel techniques described also may be used for the monitoring of stroke patients. A critical improvement to the treatment and management of patients who had suffered a stroke is the ability, provided by the novel techniques, to monitor the brain metabolism locally and continuously.

[0082] Another application involves cerebral monitoring of cardiac surgery patients. Often, cardiac surgery patients undergoing by-pass surgery have cerebral injury due to surgery. Using traditional techniques for cerebral monitoring, like invasive methods such as Licox probes are limited because patients having bypass surgery are placed on heparin (a blood thinner) at surgery. This blood thinner induces a high risk of a brain hemorrhage. The novel techniques allow for the cerebral monitoring during bypass surgery without using invasive techniques whose side effects may aggravated by the necessary blood thinners.

[0083] Another application of the inventive techniques involves the prediction of treatment efficacy in radiation-induced fibrosarcoma (RIF) tumors. A non-contact probe having source/detector fibers on the back image-plane of a camera may be used to avoid potentially compressing the tumor and altering blood flow. The lens of the camera may be approximately 15 cm away from the tumor, allowing unobstructed illumination with the treatment light at a small angle to the perpendicular. Also, the novel techniques have use in assessing therapeutic interventions to different cancers in various organs, including the head, neck, prostate, breast and brain, for example, and in determining efficacy of drugs used to teat cancers during photodynamic therapy, well known to those skilled in the art. Also, the technique may be used to monitor or assess severity or treatment benefits of tissue damage due to stroke, trauma, cardiovascular disease and other maladies.

[0084] The optical fibers for the sources and detectors may be bounded and arranged in a two-dimensional pattern to cover the whole tumor area. The largest source detector separation was 2.5 mm. An optical filter mounted in front of the camera lens attenuated light below 650 nm, enabling blood flow to be monitored, for example, using a 630 nm illumination. The sampling time for one scanning frame (13 sources and 4 detectors) may be set at approximately 18 seconds.

[0085] DCS may be used to continuously monitor blood flow during PDT (from 15 minutes before PDT to 15 minutes after PDT). Additional measurements may be performed, for example, at times 3, 6.5 and 24 hours after PDT. Treatment efficacy may be estimated by measuring the number of days required for tumor regrowth to a volume of 400 mm^3 (Time-to-Regrowth). A linear-to-log regression may be used to estimate and test for statistically significant correlations between the blood flow responses and the treatment efficacy.

[0086] Rapid vascular occlusion during PDT compromises the tissue oxygen supply, which in turn reduces PDT efficacy. Conversely, larger reductions in relative blood flow at 3 hours after PDT demonstrate permanent vascular damage, which correlates with good treatment efficacy. Therefore, the blood flow responses to PDT can be used to predict/evaluate treatment efficacy.

[0087] The novel techniques also may have some efficacy in providing clinical measurements in the human prostrate. In particular, the novel techniques allow for a real-time diffuse optical PDT dose monitoring system for ultrasound-guided interstitial human prostate PDT by determining in-vivo tissue optical properties, photosensitizer concentration, tissue blood oxygenation, and blood flow, before, during and after PDT in human prostatic carcinoma.

What is claimed:

1. A method for determining the characteristics of tissue, comprising:

measuring blood flow rate characteristics of the tissue, wherein the blood flow rate characteristics are derived from light fluctuations caused by the tissue;

measuring blood oxygenation, oxy and deoxy-hemoglobin, hemodynamic, and scattering characteristics of the tissue, wherein the blood oxygenation, oxy and deoxy-hemoglobin, hemodynamic, and scattering characteristics are derived from transmission of light through the tissue with respect to the wavelength of light; and

determining oxygen metabolism of the tissue and changes of the tissue from the measured blood flow rate and from the measure hemodynamic and oxygenation.

2. The method of claim 1, wherein the blood oxygenation and hemoglobin characteristics are further derived as a function of a position of a source detector.

3. The method of claim 1, wherein the tissue is a portion of at least one of the following: brain, muscle, breast.

4. The method of claim 1, wherein the tissue is a portion of a tumor bearing organ including at least one of the following: head, neck, prostate, breast, and brain.

5. The method of claim 1, wherein the tissue is at least one of the following: layered and heterogenous.

6. The method of claim 1, wherein the tissue characteristics are measured during exercise.

7. The method of claim 1, wherein the tissue characteristics are measured during functional activation.

8. The method of claim 1, wherein the tissue characteristics are measured during a presence of tissue damage due to stroke.

9. The method of claim 1, wherein the tissue characteristics are measured during a presence of tissue damage due to trauma.

10. The method of claim 1, wherein the tissue characteristics are measured during a presence of tissue damage due to cardiovascular disease.

11. The method of claim 1, further comprising measuring an autocorrelation of the transmitted light with respect to a delay time to determine a decay rate of an autocorrelation function.

12. The method of claim 11, further comprising determining an extent of the movement of a blood cell in the tissue.

13. The method of claim 11, further comprising determining the velocity of the movement of a blood cell in the tissue.

14. The method of claim 11, further comprising determining a motion of cell organelles in the tissue.

15. The method of claim 11, further comprising determining fluctuations of cell organelles in the tissue.

16. The method of claim 1, wherein the blood flow rate and the oxygenation are measured substantially simultaneously.

17. The method of claim 1, further comprising monitoring peripheral vascular disease.

18. The method of claim 1, further comprising monitoring therapeutic interventions to cancers in organs.

19. The method of claim 1, further comprising monitoring effects of cardiovascular disease on muscles.

20. The method of claim 1, further comprising monitoring effects of cerebrovascular disease on brain well-being and function.

21. The method of claim 1, further comprising determining an efficacy of exercise rehabilitation.

22. The method of claim 1, further comprising determining an efficacy of cancer therapy.

23. The method of claim 1, further comprising determining an efficacy of tumor treatment and therapy.

24. The method of claim 1, further comprising monitoring peripheral vascular disease.

25. The method of claim 1, further comprising determining efficacy of a drug used to facilitate blood flow.

26. The method of claim 1, further comprising determining efficacy of a drug used to treat cancers during photodynamic therapy.

27. The method of claim 1, wherein the tissue is human.

28. The method of claim 1, wherein the tissue is animal.

29. The method of claim 1, wherein the measurements are taken without a probe penetrating scalp and skull of the brain.

30. The method of claim 1, wherein the measurements are taken non-invasively.

31. A device for determining the characteristics of deep tissue, comprising:

a light source for applying light to the tissue;

a light detector for detecting the quantity of light transmitted through the tissue; and

a computer processor in communication with the light detector, wherein the computer processor determines changes in oxy . . . from changes in the transmitted light and light fluctuations as a function of wavelength to determine blood oxygenation.

32. The device of claim 31, wherein the light source is a laser.

33. The device of claim 31, wherein the light source is a stable light source.

34. The device of claim 31, further comprising optical switches to share source positions.

35. The device of claim 31, further comprising electrical switches to share detectors.

36. The device of claim 31, further comprising at least one of the following:

photodiodes, avalanche photodiodes, photomultiplier tubes, and CCD camera.

37. The device of claim 31, further comprising another laser source to measure blood flow in more than one wavelength.

38. The device of claim 31, wherein a fast CCD camera or photomultiplier is used as a detector.

39. The device of claim 31, further comprising a computer having a computer-readable medium with computer-executable instructions, wherein the computer-executable instructions calculate a correlation function.

40. The device of claim 31, further comprising a component to measure flow of externally injected microspheres through vasculature.

41. The device of claim 31, further comprising at least one other light detector.

42. The device of claim 31, wherein the device measures at least one of the following: blood oxygenation, oxy and deoxy-hemoglobin, hemodynamic, and scattering.

43. The device of claim 31, wherein the device determines oxygen metabolism.

44. The device of claim 31, wherein oxygen metabolism is measured using at bulk overall value technique.

45. The device of claim 31, wherein oxygen metabolism is measured at one or more locations.

46. The device of claim 31, wherein oxygen metabolism is measured as two dimensional imagers.

47. The device of claim 31, wherein oxygen metabolism is measured as three dimensional imagers.

* * * * *

专利名称(译)	组织血流，血流动力学和氧合的光学测量		
公开(公告)号	US20060063995A1	公开(公告)日	2006-03-23
申请号	US11/106390	申请日	2005-04-13
[标]申请(专利权)人(译)	宾夕法尼亚大学		
申请(专利权)人(译)	宾夕法尼亚大学的受托人		
当前申请(专利权)人(译)	明尼苏达大学的学者		
[标]发明人	YODH ARJUN G GREENBERG JOEL H YU GUOQIANG DETRE JOHN A DURDURAN TURGUT BURNETT MARK G MOHLER EMILE R III QUON HARRY HAHN STEPHEN M		
发明人	YODH, ARJUN G. GREENBERG, JOEL H. YU, GUOQIANG DETRE, JOHN A. DURDURAN, TURGUT BURNETT, MARK G. MOHLER, EMILE R. III QUON, HARRY HAHN, STEPHEN M.		
IPC分类号	A61B5/00 A61B5/02		
CPC分类号	A61B5/0059 A61B5/02028 A61B5/0261 A61B5/14551 A61B2562/046 A61B5/4519 A61B2562/0233 A61B2562/0242 A61B5/14553		
优先权	60/561758 2004-04-13 US		
其他公开文献	US8082015		
外部链接	Espacenet USPTO		

摘要(译)

本发明的一个实施例包括用于确定深部组织特征的装置，系统和方法。该新方法包括测量组织的血流速率和氧合特性，并根据测量血液流速和测量氧合作用确定组织的氧代谢。吹气流速特性是作为由组织引起的光波动的函数来测量的，而氧合特性是作为相对于光的波长通过组织的光传输的函数来测量的。组织可以是分层组织，例如，脑的一部分。可以在不同水平的运动强度的时间期间测量组织特征。

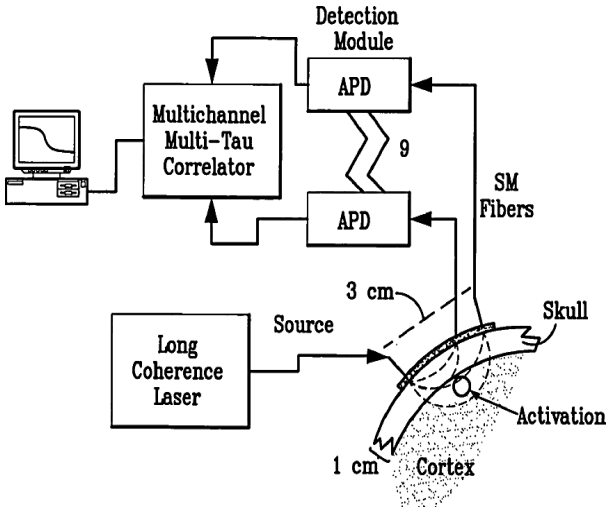
Detection
Module
APD
Multichannel
Multi-Tau
Correlator
9
APD
SM
Fibers
3 cm
Skull
Source
Long
Coherence
Laser
Activation
1 cm
Cortex